Magnetic excitations beyond the single- and double-magnons

Hebatalla Elnaggar, Abhishek Nag, Maurits Haverkort, Mirian Garcia-Fernandez, Andrew Walters, Ru-Pan Wang, Ke-Jin Zhou, Frank de Groot

Title

Magnetic excitations beyond the single- and double-magnons

Author list

Hebatalla Elnaggar,[1,2]* Abhishek Nag,[3] Maurits W. Haverkort,[4] Mirian Garcia-Fernandez,[3] Andrew Walters,[3] Ru-Pan Wang,[1,5] Ke-Jin Zhou,[3]* Frank de Groot[1]*

Affiliations

[1]Debye Institute for Nanomaterials Science, Utrecht University, 3584 CA Utrecht, The Netherlands.

[2]Institute of Mineralogy, Physics of Materials and Cosmochemistry, CNRS, Sorbonne University, 4 Place Jussieu, 75005 Paris, France.

[3]Diamond Light Source, Harwell Campus, Didcot OX11 0DE, United Kingdom.

[4]Heidelberg University, Philosophenweg 19, 69120 Heidelberg, Germany.

[5]Department of Physics, University of Hamburg, Luruper Chaussee 149, G610, 22761 Hamburg, Germany.

Abstract

A photon carrying one unit of angular momentum can change the spin angular momentum of a magnetic system with one unit ($\Delta M_s = \pm 1$) at most. This implies that a two-photon scattering process can manipulate the spin angular momentum of the magnetic system with a maximum of two units. Herein we describe a triple magnon excitation in α-Fe_2O_3, which contradicts this conventional wisdom that only 1- and 2-magnon excitations are possible in a resonant inelastic x-ray scattering experiment. We observe an excitation at exactly three times the magnon energy, along with additional excitations at four and five times the magnon energy, suggesting quadruple and quintuple magnons as well. Guided by theoretical calculations, we reveal how a two-photons scattering process can create exotic higher-rank magnons and the relevance of these quasiparticles for magnon-based applications.

Introduction

Understanding how to control the spin degree of freedom is a cornerstone for several hot topics of contemporary magnetism research, including ultrafast magnetism and magnonics. The main idea behind magnonics is to use the elementary magnetic excitations (magnons) for information transfer and processing. Magnons are bosonic quasiparticles and are the quanta of magnetic oscillations of systems with periodically ordered magnetic moments (1). A magnon is classically depicted as a phase-coherent precession of microscopic vectors of magnetization in a magnetic medium. When a magnon propagates through a magnetic medium, no electrical charge transport is involved and hence no electrical losses take place. This is the key advantage of using magnons as information carriers. The energy of magnons range typically in the terahertz range (in the order of 1 to 25 THz, i.e., 5 to 100 meV). The magnon frequency has an important impact on the performance of magnon-based devices because the larger the excitation frequency, the faster are the magnons, at least for a fraction of the magnon band. This means that the use of high-frequency (terahertz) magnons could provide a great opportunity for the design of ultrafast devices (2). Antiferromagnets represent an appealing playground for the search for new channels of high frequency, long-lived magnons paving the way towards ultrafast magnon-based devices (3,4).

Collective excitations such as magnons can be effectively measured using *2p3d* resonant inelastic x-ray scattering (RIXS) (5). Here a *2p* core electron is resonantly excited from its initial state to the empty *3d* orbitals through an electrical dipole transition. This excited state contains a localized core-hole that has a life time of ~100 fs determined by Auger decay. The radiative decay of a *2p*

core hole brings the system back to the ground state, as well as final states including low-energy excitations. In 1998, it was proposed that *2p3d* RIXS can be used to measure magnetic excitations, referred to as spin-flip by de Groot and coworkers (5). Consider a magnetic $3d^9$ system where the hole resides in the dz^2 orbital and is spin-up. An incoming photon with the correct energy and polarization can excite a *2p* core-electron into the empty dz^2 spin-up hole leading to a $2p^53d^{10}$ intermediate state. While the spin-orbit interaction at the *3d* shell is in the order of 100 meV, it is ~ 12 eV for the *2p* shell: This implies that spin and orbital momenta are mixed in the intermediate state, so neither is a good quantum number and only the total angular momentum is defined. Therefore, the intermediate state can decay to a $3d^9$ with a dz^2 spin-down hole final state. This excitation is referred to as a spin-flip excitation because when one compares the initial state with the final state, one finds that the only change between both is the spin projection from up to down and a corresponding counter change in the photon angular momentum. In a magnetic material such as α-Fe_2O_3, the magnetic excitations are nonlocal collective excitations in the form of magnons. A magnon excitation is commonly interpreted to originate from a local single-site spin-flip RIXS process. This description is widely used because the intermediate state in a *2p3d* RIXS experiment is strongly localized due to the *2p* core-hole and hence such a local picture is very useful to describe many aspects of the RIXS process. However, the final state excited by RIXS is not necessarily localized and can be a collective excitation such as magnons in a magnetic material. The way to reconcile both the local single-site and collective aspects of RIXS is to realize that the incident photon can be scattered at any equivalent site, leading to a final state that is a superposition of spin-flips at equivalent sites. Such a final state carries a nonlocal magnetic excitation and represents the magnon density of states as also confirmed by detailed comparison to inelastic neutron scattering (INS) data (6). As a photon in the x-ray regime has a non-negligible linear momentum, one can also measure the dispersion of magnons when spin-flip scattering is allowed in RIXS. This realization has been the main motivation behind the development of high resolution resonant inelastic x-ray scattering (RIXS) beamlines, with the goal to study the spin dynamics of (pseudo)spin S = ½ materials such as cuprates and iridates (7-10).

Spin-half systems represent a special case as only transitions from M_s = -½ to M_s = ½ are allowed on a single atomic site. These magnons propagate a change of one unit of angular momentum and are similar to the magnons observed by other techniques such as INS and Raman scattering (11). We will refer to these magnons as conventional single-magnons. Whereas it is only possible to flip a single spin at a local single magnetic site for cuprates and iridates resulting in a collective single-magnon excitation in the material, the nickelates can theoretically present single and double spin-flip excitations. This is because the Ni^{2+} is $3d^8$ with S = 1 and hence excitations between M_s = 1, 0, -1 are possible on a single site leading to single- and double-magnons in the extended system. RIXS measurements on NiO has confirmed the presence of single (ΔM_s = 1) and double-magnons ΔM_s = 2) in the system (12,13). We point out that double-magnons are different from bimagnons observed in cuprates. A double-magnon is a ΔM_s = 2 transition, while a bimagnon is composed of two single-magnons, one changing the spin projection with +1 (i.e., ΔM_s = 1) and the other with -1 (i.e., ΔM_s = -1) giving rise to a combined ΔM_s = 0 transition (14).

While it is clear that for high spin Ni^{2+} ions in NiO possessing two unpaired *3d* electrons that only two spins can change their angular momenta (i.e., excitations between M_s = 1, 0, -1), the situation is more complicated for a high spin $3d^5$ ion in a magnetic system. In this case, there are conceptually five spins that could be locally reversed resulting in magnons carrying a change of angular momentum of up to 5 units in the extended system (i.e., local spin-flip excitations between M_s = 5/2, 3/2, ½, -½, -3/2, 5/2 leading to a higher-rank magnon final state that is a superposition of higher-rank spin-flips at equivalent sites). This raises the fundamental question: Is it possible to change the spin angular momentum of a system with an amount greater than the change in the x-ray photon angular momentum of the RIXS experiment?

Here we provide experimental data capable of answering this question by measuring the low-energy magnon spectrum of an α-Fe_2O_3 single crystal at the ultra-high resolution I21 RIXS setup (ΔE= 32 meV) at Diamond Light Source (15). Guided by theory, we show that the crystal lattice acts as a reservoir of angular momentum which provides the extra angular momentum required to excite the higher-rank magnons (i.e., beyond single- and double-magnons). We developed a low-energy effective operator that describes the higher-rank magnons and derived simple selection rules that can be used to predict the best experimental settings for exciting the higher-rank magnons.

Results

The antiferromagnet α-Fe_2O_3 is an ideal material to initiate this kind of study because the ground state of Fe^{3+} has the maximum number of unpaired electrons for the *d* orbitals providing a platform to test the maximum number of possible single-site spin-flip excitations. Furthermore, the $^6A_1$ orbital singlet ground state makes a clean case to study solely spin excitations without any orbital contribution.

Figure 1(a) shows the Fe ions in the unit cell of α-Fe_2O_3. The exchange coupling is dominantly antiferromagnetic with the Néel temperature T_N of ~950 K. In addition to the Néel transition, α-Fe_2O_3 exhibits another magnetic transition, referred to as the Morin transition (T_M of ~250 K) where below T_M it is purely antiferromagnetic. We performed our measurements at 13 K ($T < T_M$) in the collinear antiferromagnetic phase. An exemplary L_3 x-ray absorption spectrum (XAS) is shown in Figure 1(b) where we find two main peaks (labelled E_1 and E_2 where this splitting is due to the crystal field) exhibiting the expected x-ray magnetic linear dichroism signal in line with previous literature (16-18).

The RIXS spectrum measured at E_1 is shown in Figure 1(c). The elastic line is observed at zero energy transfer where the final state preserves the initial state spin orientation. A cascade of energy transfer peaks can be seen at 100, 200, 300, 400 and 500 meV. The first energy transfer peak can be assigned to a single-magnon excitation. This agrees well with the observation from INS experiments, where an optical nearly non-dispersing mode is observed at ~100 meV (19). The single-magnon excitation propagates a change of angular momentum of $\Delta M_s = 1$. The second energy transfer peak appears at double the energy of the single-magnon and can be assigned to a double-magnon excitation ($\Delta M_s = 2$) similar to the double-magnon excitation observed in NiO (12,13). The most remarkable feature in our results is the ability of the two-photon RIXS process to excite higher-rank magnons at 3 times, 4 times and potentially at 5 times the energy of a single-magnon (zoom in Figure 1(d) and its first derivative in (e)). These higher-rank magnons propagate these multiples of angular momentum. We provide the details of the fitting and the full energy loss spectra at two incident energies in the materials and methods in Figures S1, S2 and S3.

We measured the angular dependence of the single-, double- and triple-magnons by rotating the sample in the azimuthal (α) direction to decipher the nature of the transitions involved (see Figure 2). Conceptually, one expects that the angular behavior of the higher-order magnons differs from the single-magnon as the angular momentum selections rules are different ($\Delta M_s = 1, 2, 3$ involves a dipolar, quadrupolar and hexapolar spin-flip process respectively). This is confirmed by comparing the angular behavior in panels (a), (b) and (c) of Figure 2 where the magnitudes of the transitions are reduced approximately with an order of magnitude as we move from single- to double- to triple-magnons, in addition to the change of the angular profile. The angular dependent RIXS of these excitations however, did not show any noticeable dispersion (see Figure S4). The parent single-magnon is an optical mode that shows negligible dispersion according INS measurements which agrees with our measurement (19).

Discussion

The implication of our experimental observation is that the two-photon RIXS process can exchange five units of angular momenta with a single magnetic-site. This is an unexpected result because the selection rule for a dipole transition in presence of strong spin-orbital coupling is that the change of the total angular momentum (ΔM_j) is equal to 0 or ±1. This means that for a dipole-in (*2p* → *3d* transition), dipole-out (*3d* → *2p* transition) *2p3d* RIXS process, possible transition should involve ΔM_j = 0, ±1, ±2 giving rise to only single- and double-magnons. We performed multiplet ligand field theory calculations for Fe^{3+} L_3-edge RIXS (see Figure 3(a)) which confirms that only single- and double- magnons are expected to be observed and is in line with previous work on NiO (12,13). It is essential to examine the interaction terms of the model Hamiltonian responsible for the single- and double-magnons to find the origin behind the higher-rank magnons in α-Fe_2O_3.

$$H = \sum_k f_k F^k + \sum_k g_k G^k + \sum_i l_i . s_i + J_{exch}(n.S) \quad (1)$$

The model Hamiltonian used for the calculation is given by equation (1). The $J_{exch}(n.S)$ term is the mean-field super exchange interaction term that determines the energy of the single-magnon. The spin orbit coupling is given by the $\sum_i l_i . s_i$ term and is responsible for the spin-flip process by mixing the orbital and spin degrees of freedom and enables the observation of single-magnons as detailed in the work of de Groot *et. al.* (5). The double-magnon is enabled through the intra-atomic Coulomb exchange given by $\sum_k f_k F^k + \sum_k g_k G^k$. F_k(f_k) and G_k(g_k) are the Slater–Condon parameters for the radial (angular operators) part of the direct and exchange Coulomb interactions, respectively. The intra-atomic Coulomb exchange interaction strongly couples the valence and core electrons implying that the spin angular momentum of both the core and valence orbitals are no longer a good quantum number, effectively leading to ΔM_s = 0, 1, and 2 excitations.

It is inevitable to conclude that the higher-rank magnons have a different origin compared to the single- and double-magnons reported in previous work (12, 13, 20) and a mechanism that allows the exchange of higher angular momenta is needed. This apparent contradiction can be reconciled by realizing that the angular momenta of electrons only is not a conserved quantum number in real crystals (21). The crystal lattice can exchange angular momentum with the electrons providing the extra angular momentum required for higher-rank magnons involving $\Delta M_s > 2$. We performed a full-multiplet ligand field theory calculation for Fe^{3+} L_3-edge RIXS including the effect of the crystal lattice using an effective octahedral crystal field potential (see Figure 3(b)). In addition to the single- and double-magnons, triple-, quadruple- and quintuple-magnons are now visible confirming that the crystal field potential is the key factor behind the higher-rank excitations as can be seen in details in the linear cuts of the RIXS map in Figure 3(c). Here we stress that the higher-rank magnons are generated from a single magnetic-site and the role of the crystal lattice can be considered as a reservoir of angular momentum supplying the extra angular momentum required.

To visualise the role of the crystal lattice, we follow in Figure 4 the fate of an excitation created by the absorption, for example, of a circular right polarized photon. We define the polarization of light as: $|R\rangle = \frac{1}{\sqrt{2}}[1, -i, 0]$, $|L\rangle = [1, i, 0]$ and $|Z\rangle = [0,0,1]$. The initial state can be represented by the vector shown in Figure 4(a) which includes the *2p* and *3d* orbitals participating in the RIXS process. The first two numbers shaded in gray represent the occupation of the *2p* spin down (red arrow) and *2p* spin up orbitals (blue arrow) where we take the spin quantization axis to be the C_4 axis of the octahedron. The second two numbers shaded in yellow are the *3d* spin down (red arrow) and *3d* spin up orbitals (blue arrow) occupation numbers. The projection of the total orbital angular

momentum, L_Z, is specified in the subscript of the vector to keep track of the orbital angular momentum of the states. This means that the initial state is given by $(3,3,5,0)_0$.

Upon the absorption of the polarized photon, a spin-up electron can be excited from the *2p*$_{-1}$ to the *3d*$_{-2}$ orbital resulting in an intermediate state given by $(3,2,5,1)_{-1}$ (Figure 4(a)). This intermediate state can decay back elastically by emitting a right polarized photon contributing to the elastic RIXS peak (Figure 4(b1)). Another possible path is shown in Figure 4(b2) where a $3d_{-2}^{\uparrow}$ electron scatters off the crystal field potential to a $3d_{2}^{\uparrow}$ orbital and thereby changes its angular momentum by four units. This extra angular momentum provided by the lattice is the key aspect that makes it possible to excite higher-rank magnons. A cascade of *2p* spin-orbit coupling and *2p-3d* exchange interaction are required to transfer this orbital angular momentum to spin angular momentum as illustrated in panels (c) to (i) of Figure 4. The first pair of *2p* spin-orbit coupling and *2p-3d* exchange interaction changes the intermediate state to $(3,2,4,2)_2$. We note that this intermediate state cannot decay to a single-magnon excitation as it cannot reach a $L_Z = 0$ final state through a dipole emission. The second pair of *2p* spin-orbit coupling and *2p-3d* exchange interaction changes the intermediate state to $(3,2,3,3)_1$. Now this intermediate state can decay to a double-magnon excitation either after the *2p* spin-orbit coupling step ($2p_{-1}^{\downarrow} \rightarrow 3d_{-2}^{\downarrow}$ emitting a left polarized photon - not shown in Figure 4 for visual clarity) or after the exchange interaction step emitting a left polarized photon (Figure 4(g1)). A final *2p* spin-orbit coupling step is required to changes the intermediate state to $(2,3,3,3)_0$ which can finally decay to a triple-magnon by emitting a Z polarized photon (Figure 4(h)).

Quadruple and quintuple magnons can be reached by further exchange of angular momentum with the lattice followed by cascades of *2p* spin-orbit coupling and *2p-3d* exchange interaction. In contrast, when the crystal-field is not considered, only single- and double-magnons can be excited (see the Feynman-diagrams in Figure S5). The transparent Feynman-diagram representation allows us to derive simple selection rules for this example: (i) it is not possible to excite single-magnons using circular right polarized incoming x-rays, (ii) double-magnons can be selectively observed by detecting the left polarized outgoing light. (iii) triple-magnons can be selectively observed by detecting the Z polarized outgoing light. The Z polarized light can be experimentally detected by placing an extra detector in the vertical plane for example. A full RIXS calculation is shown in Figure S6 and confirms the selection rules derived from Figure 4.

We developed a low-energy effective RIXS operator that describes low-energy magnetic excitations such as magnons in terms of spin operators based on the work of Haverkort (22). The full RIXS cross-section is given by equation (2) where the ground state $|i\rangle$ is excited by a photon described by a dipole transition operator T_{ϵ_i} to an intermediate state described by the Hamiltonian (H) and decays to all possible final states $|f\rangle$ emitting a photon described by a dipole transition operator T_{ϵ_o}.

$$RIXS(\omega) \propto \sum_f |\langle f|T_{\epsilon_o}^{\dagger} \frac{1}{\omega_i - H + i\Gamma/2} T_{\epsilon_i}|i\rangle|^2 = \sum_f |\langle f|R_{eff}|i\rangle|^2 \quad (2)$$

The effective operator (R_{eff}) removes the intermediate state from the equation by expanding the intermediate state Hamiltonian in terms of polynomials of spin operators multiplied by x-ray absorption fundamental spectra. The expression of the expansion to the third order is presented in the materials and methods and is summarized in Figure 5(a). The spin flip processes resulting in magnons can be grouped in order of the spin operator rank: linear (shaded in blue), quadratic (shaded in purple) and cubic (shaded in red) operators. The linear spin operators can generate single-magnons while the quadratic spin operators generate single- and double-magnons and

produce the majority of the RIXS intensity (see Figure 5(b)). Finally, the cubic spin operators can generate single-, double- and triple-magnons. The main advantage of this expansion is its simple form that allows one to determine general selection rules depending on the polarization of the incoming and outgoing light.

We computed the angular dependence of the single-, double- and triple-magnons based on this expansion in Figure 6. Our calculations capture the essential aspects of the experimental angular dependence where we obtain the correct order of magnitude for the magnons and reproduce the general angular dependence confirming the nature of the higher-rank magnons (compare Figure 2 to Figure 6). Some deviations of the calculated angular dependence from the experiment could be to several factors. On the experimental side, our measurements were performed on a bulk single crystal which is prone to self-absorption and saturation effects. As the RIXS cross-section is a combination of an absorption (photon-in) process and an emission (photon- out) process, two geometrical effects have to be taken into account here: the probing depth is dependent on the x-ray absorption spectroscopy (XAS) cross-section (saturation) and the emitted photons can be re-absorbed (self-absorption). Consequently, the RIXS intensity is distorted in a bulk crystal according to the photon energy and the experimental geometry (23). When the sample is rotated, the probing depth is changed, and the photons emitted at different energies have different escape lengths, hence distorting the angular dependence. It is difficult to correct for these geometrical energy-dependent effects because it is affected by the background absorption (which is the off-resonant contribution from other elements in the sample and in the path of the beam). On the theoretical side, one likely reason for the deviation could be the fact that the Fe sites in hematite have a small trigonal distortion. As a first approximation, the trigonal distortion would not change the ground state of Fe^{3+} because the singlet $^6A_1$ ground state does not split. However, the trigonal distortion would influence the intermediate states, and hence could modify the intensity and consequently the angular dependence (24). Finally, we point out that ligand field-multiplet theory reduces a full solid to a local cluster. This means that any Fe-Fe interactions or intercluster hopping are not considered. We expect that the above approximations can affect the angular dependence (25).

The comparison between theory and experiment on α-Fe_2O_3 confirms that the cascade of excitations we observed at triple, quadruple, and quintuple the energy of a single-magnon are higher rank-magnons that propagate these higher multiples of spin angular momentum. From a fundamental point of view, the higher-rank magnons can couple differently with the various degrees of freedom of the system providing a unique platform to investigate magnon interactions. From a technological point of view, these excitations have higher energies than that of single-magnons and hence are potentially more thermally robust. We predict that these higher-rank magnons can also be excited using THz-pulses and can be enhanced using magnonic crystals paving the way towards future magnonic devices.

Methods

Resonant inelastic x-ray scattering measurements

High-resolution (ΔE= 32 meV), Fe L_3-edge resonant inelastic x-ray scattering measurements were done at the I21 beamline of the Diamond Light Source, United Kingdom. Linear horizontally (π) or vertically polarized (σ) x-ray beam was used. The angular dependence was measured by rotating the sample about the b-axis (referred to as α rotation) of a polished α-Fe_2O_3 single crystal cooled down to 13 K. The Morin temperature of Fe_2O_3 is 220 K. The scattering angle was kept fixed at 150°. The x-ray absorption spectrum (XAS) shown in Figure 1(b) was measured using total electron yield in the same geometry. The pressure in the experimental chamber was maintained below $5x10^{-10}$ mbar. The zero-energy transfer position and resolution of the RIXS spectra were determined from subsequent measurements of elastic peaks from an adjacent carbon tape.

Resonant inelastic x-ray scattering data fitting

RIXS data were corrected for self-absorption prior to fitting. The elastic line was fitted with an energy resolution limited Gaussian lineshape (orange shade, Figure 1(c) and SI Figure 1(a)). The phonon peaks close to 43 meV and 150 meV were fitted with asymmetric Lorentzian functions (shown by gray dashed lines) convoluted with the energy resolution. These peaks are clearly visible in RIXS spectra at E_2 peak of XAS (see inset of SI Figure 1(b)). The five shaded antisymmetric Lorentzian peaks convoluted with the energy resolution represent the single- (blue), double- (purple), triple- (red), quadruple- (green) and quintuple- (black) magnon excitations (Figure 1c and SI Figure 1(a)). While the energy positions up to the quadruple magnon excitation were kept as a free parameter for fitting, the energy position of the quintuple magnon was fixed to (fitted energy position of the triple magnon)*(5/3). See also SI Figure 2 and SI Figure 3 for the low energy fits to the RIXS data for different α at π and σ polarisations, respectively.

Multiplet ligand-field calculations

The crystal field multiplet model is an effective model Hamiltonian for the description of all charge conserving excitations of ionic transition metal systems. The crystal field multiplet model is valid for the main peaks of *2p* x-ray absorption and the low-energy RIXS excitations of ionic transition metal ions, because the *2p3d* x-ray absorption and the *3d2p* x-ray emission are neutral, self-screened, transitions, which implies that screening channels such as ligand-metal charge transfer can be approximated by renormalized parameters. We used the quantum many-body program Quanty (26) to simulate Fe XAS and *2p3d* RIXS in α-Fe_2O_3. The Hamiltonian used for the calculations consists of the following terms: (i) Coulomb interaction, (ii) crystal field potential, (iii) spin−orbit coupling, and (iv) effective exchange interaction. The $d-d$ ($p-d$) multipole part of the Coulomb interaction was scaled to 70% (80%) of the Hartree−Fock values of the Slater integral. The general parameters used for the simulations agree with previous studies of α-Fe_2O_3 $L_{2,3}$ edges.

Expression of the effective RIXS operator

The effective operator can be expressed by equation (3) as shown by Haverkort (22). Here $\epsilon_{in(out)}$ is the incoming (outgoing) polarization of the photons. $F_{\{x,y,z\}}$ is the conductivity tensor describing the full magneto-optical response function of the system depending on the local magnetization direction given by $\{x, y, z\}$.

$$R_{eff} = -\mathrm{Im}[\epsilon_{in}^{*} \cdot F_{\{x,y,z\}} \cdot \epsilon_{out}] \tag{3}$$

The general form of the conductivity tensor can be expressed as a sum of linear independent spectra multiplied by functions depending on the local magnetization direction as given in equation (4).

$$F_{\{x,y,z\}} = \sum_{k=0}^{\infty} \sum_{m=-k}^{k} \begin{pmatrix} F_{xx}^{k,m} & F_{xy}^{k,m} & F_{xz}^{k,m} \\ F_{yx}^{k,m} & F_{yy}^{k,m} & F_{yz}^{k,m} \\ F_{zx}^{k,m} & F_{zy}^{k,m} & F_{zz}^{k,m} \end{pmatrix} Y_{k,m}(\theta, \phi) \tag{4}$$

Here θ and ϕ define the direction of the local moment with θ being the polar angle, and ϕ being the azimuthal angle. $Y_{k,m}(\theta, \phi)$ is a spherical harmonic function and $F_{ij}^{k,m}$ is the *i*,*j* component of the conductivity tensor on a basis of linear polarized light in the coordinate system of the crystal. In symmetries lower than spherical, this expansion on spherical harmonics does not truncate at finite k and the angular momentum of the electrons only is not a conserved quantum number in the crystals. We have shown in our previous work that including terms up to $k = 3$ is sufficient to describe Fe^{3+} ions in octahedral crystal field (27). The expression is given in equation (5) and involves terms up to the 3rd order in spin leading to single, double, and triple spin flip processes.

$$F_{\{x,y,z\}} = \begin{pmatrix} F^0_{a1g} + 2F^2_{eg}({S_x}^2 - \frac{1}{3}S^2) & F^2_{t2g}(S_xS_y + S_yS_x) - F^1_{t1u}Sz - F^3_{t1u}(-\frac{3S_z}{5} + {S_z}^3) & F^1_{t1u}S_y + F^3_{t1u}(-\frac{3S_y}{5} + {S_y}^3) + F^2_{t2g}(S_xS_z + S_zS_x) \\ F^2_{t2g}(S_y + S_yS_x) + F^1_{t1u}Sz + F^3_{t1u}(-\frac{3S_z}{5} + Sz^3) & F^0_{a1g} + 2F^2_{eg}({S_y}^2 - \frac{1}{3}S^2) & -F^1_{t1u}S_x - F^3_{t1u}(-\frac{3S_x}{5} + {S_x}^3) + F^2_{t2g}(S_yS_z + S_zS_y) \\ -F^1_{t1u}S_y - F^3_{t1u}(-\frac{3S_y}{5} + {S_y}^3) + F^2_{t2g}(S_xS_z + S_zS_x) & F^1_{t1u}S_x + F^3_{t1u}(-\frac{3S_x}{5} + {S_x}^3) + F^2_{t2g}(S_yS_z + S_zS_y) & F^0_{a1g} + 2F^2_{eg}({S_z}^2 - \frac{1}{3}S^2) \end{pmatrix} \quad (5)$$

Data availability

The data generated and analyzed are included in the paper and its supplementary information and have been all deposited in the zenodo database under accession code at https://zenodo.org/record/7828290. Raw data files will be made available upon request.

Code availability

The code that supports the findings of this study is available online and can be downloaded at: https://www.quanty.org together with a full documentation and instructions to use it. The script file required to reproduce the theoretical figures has been deposited in the zenodo database under accession code at https://zenodo.org/record/7828290.

References

1. F. Bloch, Zur Theorie des Austauschproblems und der Remanenzerscheinung der Ferromagnetika. *Z. Phys.* **74**, 295-335 (1939).
2. K. Zakeri, Terahertz magnonics: Feasibility of using terahertz magnons for information processing. *Phys. C: Supercond. Appl.* **549**, 164-170 (2018).
3. A. Safin, S. Nikitov, A. Kirilyuk, D. V. Kalyabin, A. Sadovnikov, P. Stremoukhov, M. Logunov, P. Popov, Excitation of terahertz magnons in antiferromagnetic nanostructures: Theory and experiment. *J. Exp. Theor. Phys* **131**, 71-82 (2020).
4. V. Kruglyak, S. Demokritov, D. Grundler, Magnonics. *J. Phys. D: Appl. Phys*. **43**, 260301 (2010).
5. F. de Groot, P. Kuiper, and G. Sawatzky, Local spin-flip spectral distribution obtained by resonant x-ray Raman scattering, *Phys. Rev. B.* **57**, 14584 (1998).
6. L. Ament, M. van Veenendaal, T. Devereaux, J. Hill, J. van den Brink, Resonant inelastic x-ray scattering studies of elementary excitations. *Rev. Mod. Phys*. **83**, 705-767 (2011).
7. M. Dean, R. Springell, C. Monney, K.-J. Zhou, J. Pereiro, I. Božović, B. Dalla Piazza, H. Rønnow, E. Morenzoni, J. van den Brink, T. Schmitt, J. Hill, Spin excitations in a single La_2CuO_4 layer. *Nat. Mater*. **11**, 850-854 (2012).
8. Y. Peng, G. Dellea, M. Minola, M. Conni, A. Amorese, D. Di Castro, G. De Luca, K. Kummer, M. Salluzzo, X. Sun, X. Zhou, G. Balestrino, M. Le Tacon, B. Keimer, L. Braicovich, N. Brookes, G. Ghiringhelli, Influence of apical oxygen on the extent of in-plane exchange interaction in cuprate superconductors. *Nat. Phys.* **13**, 1201-1206 (2017).
9. J. Kim, D. Casa, M. Upton, T. Gog, Y.-J. Kim, J. Mitchell, M. van Veenendaal, M. Daghofer, J. van den Brink, G. Khaliullin, and B. Kim, Magnetic excitation spectra of Sr_2IrO_4 probed by resonant inelastic x-ray scattering: Establishing links to cuprate superconductors. *Phys. Rev. Lett.* **108**, 177003 (2012).
10. M. Dean, Y. Cao, X. Liu, S. Wall, D. Zhu, R. Mankowsky, V. Thampy, X. Chen, J. Vale, D. Casa, J. Kim, A. Said, P. Juhas, R. Alonso-Mori, J. Glownia, A. Robert, J. Robinson, M. Sikorski, S. Song, M. Kozina, H. Lemke, L. Patthey, S. Owada, T, Katayama. M. Yabashi, Y. Tanaka, T. Togashi, J. Liu, C. Rayan Serrao, B. Kim, L. Huber, D. McMorrow, M. Först, J. Hill, Ultrafast energy- and momentum-resolved dynamics of

magnetic correlations in the photo-doped Mott insulator Sr_2IrO_4. *Nat. Mater*. **15**, 601-605 (2015).
11. H. Robarts, M. García-Fernández, J. Li, A. Nag, A. Walters, N. Headings, S. Hayden. K.-J. Zhou, *Phys. Rev.B.* **103**, 224427 (2021).
12. G. Ghiringhelli, A. Piazzalunga, C. Dallera, T. Schmitt, V.N. Strocov, J. Schlappa, L. Patthey, X. Wang, H. Berger, M. Grioni, Observation of two nondispersive magnetic excitations in NiO by resonant inelastic soft-X-ray scattering. *Phys. Rev. Lett*. **102**, 027401 1–4 (2009).
13. A. Nag, H. Robarts, F. Wenzel, J. Li, H. Elnaggar, R.-P. Wang, A. Walters, M. García-Fernández, F. de Groot, M. W. Haverkort, K.-J. Zhou, Many-body physics of single and double spin-flip excitations in NiO. *Phys. Rev. Lett.* **124**, 067202 (2020).
14. L. Chaix, E. Huang, S. Gerber, X. Lu, C. Jia, Y. Huang, D. McNally, Y. Wang, F. Vernay, A. Keren, M. Shi, B. Moritz, Z.-X. Shen, T. Schmitt, T. Devereaux and W.-S. Lee, Resonant inelastic x-ray scattering studies of magnons and bimagnons in the lightly doped cuprate $La_{(2-x)}Sr_xCuO_4$. *Phys. Rev. B.* **97**, 155144 (2018).
15. K.-J. Zhou,* A. Walters, M. Garcia-Fernandez, Th. Rice, M. Hand, A. Nag, J. Li, S. Agrestini, P. Garland, H. Wang, S. Alcock, I. Nistea, B. Nutter, N. Rubies, G. Knap, M. Gaughran, F. Yuan, P. Chang, J. Emmins and G. Howell, I21: an advanced high-resolution resonant inelastic x-ray scattering beamline at Diamond Light Source. *J. Synchrotron Rad.* **29**, 563–580 (2022).
16. P. Kuiper, B. Searle, P. Rudolf, L. Tjeng, C. Chen, X-ray magnetic dichroism of antiferromagnet Fe_2O_3: The orientation of magnetic moments observed by Fe 2p x-ray absorption spectroscopy. *Phys. Rev. Lett*. **70**, 1549-1552 (1993).
17. P. Miedema and F. de Groot, The iron L edges: Fe 2p x-ray absorption and electron energy loss spectroscopy. *J. Electron Spectros. Relat. Phenomena*, **187**, 32-48 (2013).
18. J. Miyawaki. S. Suga, H. Fujiwara, M. Urasaki, H. Ikeno, H. Niwa, H. Kiuchi, Y. Harada. Dzyaloshinskii-Moriya interaction in α-Fe_2O_3 measured by magnetic circular dichroism in resonant inelastic soft x-ray scattering. *Phys. Rev. B*, 96, 214420 (2017).
19. E. Samuelsen, G. Shirane, Inelastic neutron scattering investigation of spin waves and magnetic interactions in Fe_2O_3. *Phys. Stat. Sol.* **42**, 241-256 (1970).
20. A. Nag, A. Nocera, S. Agrestini, M. Garcia-Fernandez, A. C. Walter, S.-W. Cheong, S. Johnston, K.-J. Zhou, Quadrupolar magnetic excitations in an isotropic spin-1 antiferromagnet. *Nat. Commun.* **13**, 2327 (2022).
21. S. Streib, Difference between angular momentum and pseudoangular momentum. *Phys. Rev. Lett*. **103**, L100409 (2021).
22. M. W. Haverkort, Theory of resonant inelastic x-ray scattering by collective magnetic excitations. *Phys. Rev. Lett*. **105**, 167404 (2010).
23. R.-P. Wang, H. Elnaggar, Ch. J. Titus, K. Tomiyasu, J. Geessinck, G. Koster, F. Frati, J. Okamoto, D.-J. Huang, F. de Groot, Saturation and self-absorption effects in the angle-dependent 2p3d resonant inelastic X-ray scattering spectra of Co^{3+}. *J. Synchrotron Rad.* **27**, 1–9 (2020).
24. J. Miyawaki, S. Suga, H. Fujiwara, M. Urasaki, H. Ikeno, H. Niwa, H. Kiuchi, Y. Harada, Dzyaloshinskii-Moriya interaction in α−Fe_2O_3 measured by magnetic circular dichroism in resonant inelastic soft x-ray scattering, *Phys. Rev. B.* **96**, 214420 (2017).
25. F. de Groot, H. Elnaggar, F. Frati, R.P. Wang, M. U. Delgado-Jaime, M. van eenendaal, J. Fernandez-Rodriguez, M. W. Haverkort, R. J. Green, G. van der Laan, Y. Kvashnin, A. Hariki, H. Ikeno, H. Ramanantoanina, C. Daul, B. Delley, M. Odelius, M. Lundberg, O. Kuhn, S. I. Bokarev, E. Shirley, J. Vinson, K. Gilmore, M. Stener, G. Fronzoni, P. Decleva, P. Kruger, M. Retegan, Y. Joly, Ch. Vorwerk, C. Draxl, J. Rehr, A.Tanaka, 2p x-

ray absorption spectroscopy of *3d* transition metal systems, *J. Electron Spectros. Relat. Phenomena*, **249**, 147061 (2021).
26. M. W. Haverkort, M. Zwierzycki, O. K. Andersen, Multiplet ligand-field theory using Wannier orbitals. Phys. Rev. B **58**, 165113 (2012).
27. H. Elnaggar, M. W. Haverkort, M. H. Hamed, S. S. Dhesi and F. de Groot, Tensor description of X-ray magnetic dichroism at the Fe $L_{2,3}$-edges of Fe_3O_4. *J. Synchrotron Rad.* **28**, 247–258 (2021).

Acknowledgments

We acknowledge the staff of beamline I21 of Diamond Light Source for their help in setting up and running the experiments. We acknowledge the following fundings:
Dutch Research Council Rubicon Fellowship (Project No. 019.201EN.010): HE
ERC advanced Grant XRAYonACTIVE No. 340279: FdG

Author Contributions Statement:

Conceptualization: HE, FdG
Methodology: HE, FdG, RW, AN, KJZ
Investigation: AN, KJZ, MGF, AW
Visualization: HE, FdG, MWH
Writing—original draft: HE
Writing—review & editing: HE, FdG, MWH, KJZ

Correspondence and requests for materials should be addressed to Hebatalla Elnaggar, Ke-Jin Zhou, and Frank de Groot.

Competing Interests Statement:

The authors declare no competing interests.

Figure Legends/Captions (for main text figures):

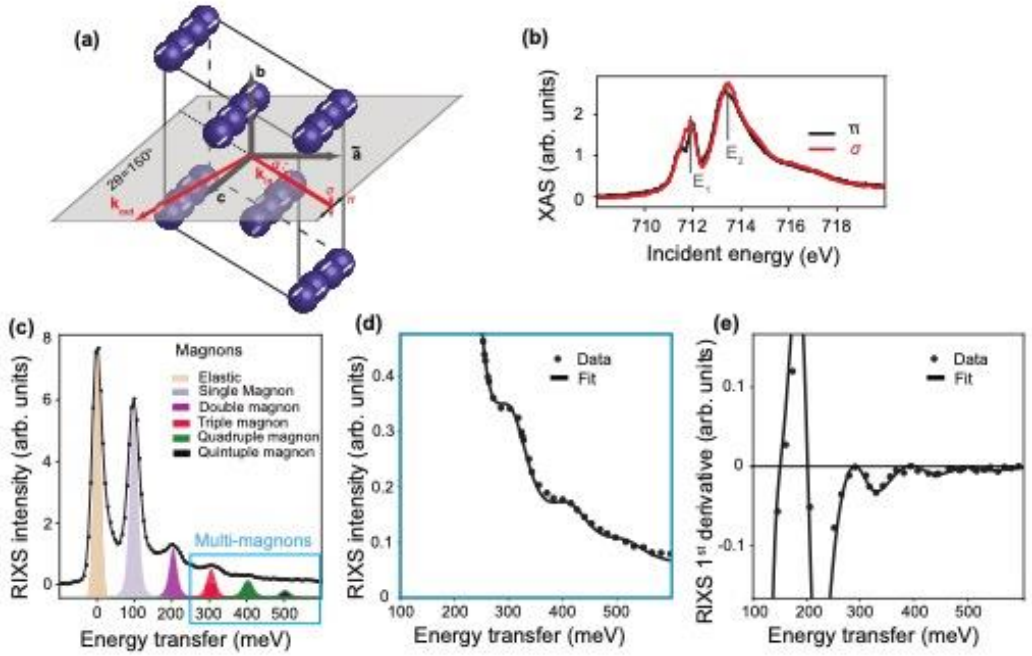

Fig. 1. Crystal structure and x-ray L_3-edge measurements in a (0001) α-Fe_2O_3 single crystal. (a) Crystal structure of α-Fe_2O_3 showing only the Fe atoms and the scattering geometry used for all measurements presented in this work. $\mathbf{k_{in(out)}}$ are the incident and outgoing wave vectors and the scattering angle (2θ) was kept fixed at 150°. The incidence angle is α with α = 90° for normal incidence. The antiferromagnetic order is depicted with white arrows showing the orientation of the magnetic moments. **(b)** Fe L_3 XAS measured with π (black) and σ (red) polarization. Two main peaks can be identified and are labelled E_1 and E_2. **(c)** RIXS spectra measured at E_1 (α = 95°, π polarization). The orange shaded Gaussian peak at zero energy transfer corresponds to the elastic peak also having contribution from ΔM_S=0 excitation. The five shaded antisymmetric Lorentzian peaks represent the single- (blue), double- (purple), triple- (red), quadrupole- (green) and quintuple- (black) magnon excitations (see Methods for the fitting details). The blue box highlights the spin non-conserving transitions. **(d)** A zoom on the spin non-conserving transitions. The dots are experimental data, and the black line is the fit. The triple- and quadrupole -magnons can be clearly identified. **(e)** The first derivative of panel **(d)** where the signal equals zero at the position of the higher-rank magnons.

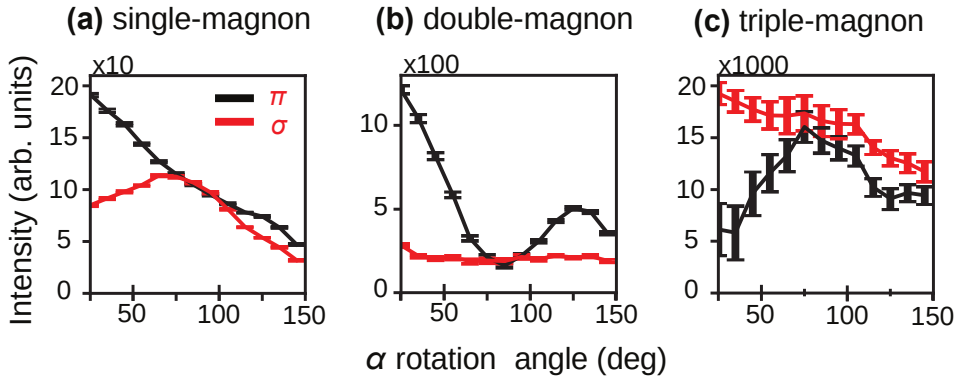

Fig. 2. Angular dependence of the magnons measured with π and σ polarization. (a) Single-magnon, **(b)** double-magnon and **(c)** triple-magnon excitations measured at the incidence energy E_1. The angular dependence is measured by rotating the single crystal in the azimuthal direction (α rotation) while the scattering angle was kept fixed at 150°. The error bars shown are least square fitted intensity value errors.

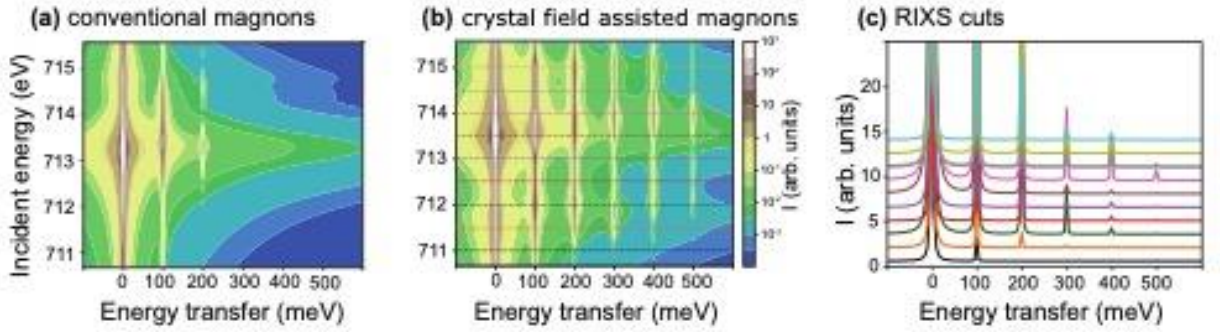

Fig. 3. Full-multiplet ligand field theory calculation for Fe^{3+} L_3-edge RIXS in α-Fe_2O_3. **(a)** Incident energy dependent RIXS intensity map for an Fe^{3+} ion according to the Hamiltonian in Equation 1. **(b)** Considering an additional term that includes the crystal field effects. The calculations were performed for linear horizontal incoming beam and unpolarized outgoing beam to correspond to the experimental conditions. The parameters used for the calculations are reported in SI Tab. 1. We note that the intensity is plotted in a logarithmic scale. **(c)** Line cuts through the RIXS map of panel **(b)** plotted at the dashed lines positions shown on the map.

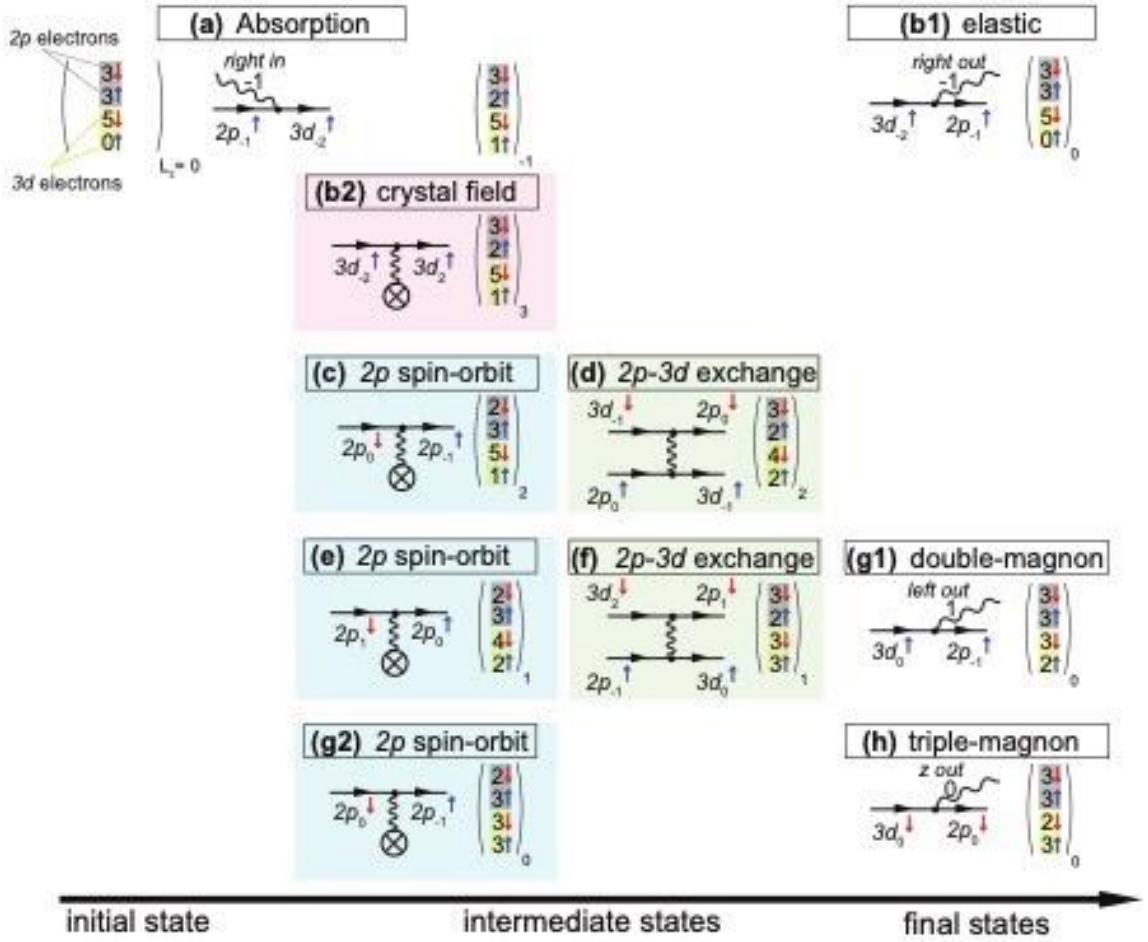

Fig. 4. Schematic representation of the mechanism of higher-rank magnons by *2p3d* RIXS. The initial state vector is shown in the upper left corner comprising of the *2p* (gray) and *3d* (yellow) orbitals participating in the RIXS process. The spin of the electrons is depicted by the colored arrows (red = down, blue = up). We follow the fate of a *2p*→*3d* excitation created by the absorption of a right polarized photon **(a)** up to the triple-magnon decay through a cascade of crystal field interaction, *2p* spin-orbit coupling and *2p-3d* exchange interaction through the steps from **(b)** to **(h)**.

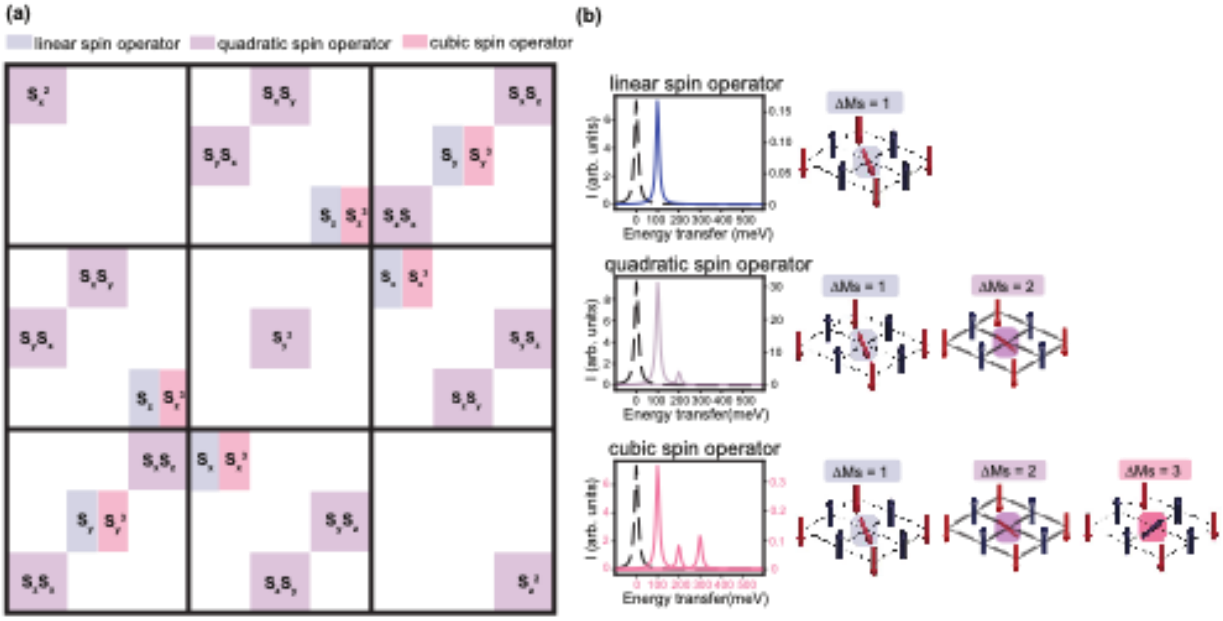

Fig. 5. Matrix elements of the effective RIXS operator (R_{eff}) expanded up to the third rank and the RIXS spectrum from individual operators. (a) A summary of the expansion presented in equation 3 grouped in terms of linear (blue), quadratic (purple) and cubic (red) spin operators (**S**) involved in the RIXS cross-section. **(b)** The RIXS cross-section computed using the three orders of the spin operators.

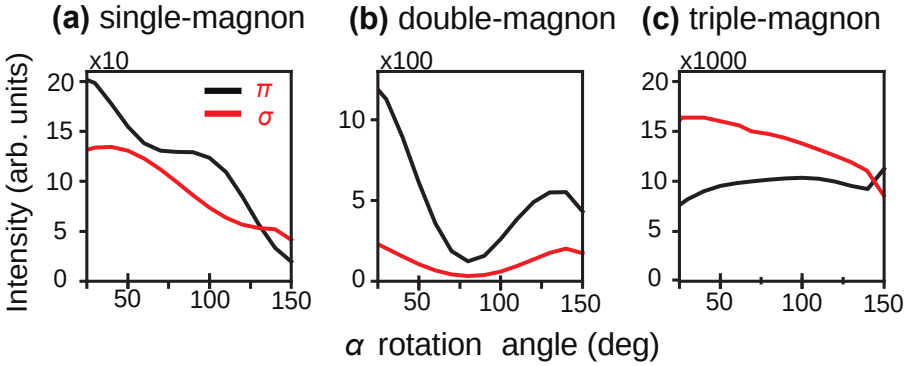

Fig. 6. Computed angular dependence of the magnons measured with π and σ polarization using the effective operator expansion. (a) Single-magnon, **(b)** double-magnon and **(c)** triple-magnon excitations at the incidence energy E_1.